Advances in Environmental Technology 10(2) 2024, 142-159.

Iranian Reasearch Organization for Science and Technology (IROST)

Advances in Environmental Technology

Journal home page: https://aet.irost.ir

Adsorption of carmoisine and malachite green on silicon dioxide-based stones nanosized by ball milling

Pegah Bahman[a], Tayebe Bagheri Lotfabad[*b], Amir Heydarinasab[a], Soheila Yaghmaei[c]

[a] *Department of Chemical Engineering, Science and Research Branch, Islamic Azad University, Tehran, Iran.*

[b] *Department of Industrial and Environmental Biotechnology, National Institute of Genetic Engineering and Biotechnology (NIGEB), Tehran, Iran.*

[c] *Department of Chemical and Petroleum Engineering, Sharif University of Technology, Tehran, Iran.*

ARTICLE INFO

Document Type:
Research Paper

Article history:
Received 28 February 2024
Received in revised form
7 May 2024
Accepted 20 May 2024

Keywords:
Synthetic Dyes
Adsorption
Wastewater
Silica
Natural Porous Materials

ABSTRACT

Industries extensively use synthetic dyes, and it is crucial to eliminate them from effluents to prevent their accumulation in nature. The elimination of synthetic dyes is effectively achieved through the well-established method of adsorption; previous researchers have developed a range of materials dedicated to the adsorption of such dyes. In this regard, natural materials have received much attention as environmentally friendly. This study examined the ability of SiO_2-based stone samples, including silica, zeolite, pumice, and scoria, to adsorb carmoisine and malachite green dyes from water. The ball-milling method was utilized to prepare the nanosized adsorbents. Physicochemical properties were evaluated by analytical methods, including dynamic light scattering (DLS), X-ray diffraction (XRD), X-ray fluorescence (XRF), Brunauer-Emmett-Teller (BET), and Fourier transform infrared spectroscopy (FTIR). The removal of dyes was experimentally undertaken utilizing both granular and nanosized adsorbents with conditions of 30°C temperature, pH 7, and initial dye concentrations set at 45 mg/l. Adsorption isotherm models and kinetic models were evaluated for dye adsorption. The highest levels of adsorption capacities for carmoisine and malachite green were 54.42 and 19.01 mg/g, respectively. The findings of this research demonstrated that nanosized scoria and silica have the potential to be used as efficient adsorbents in cationic and anionic dye removal, respectively.

1. Introduction

Extensive research has been conducted to mitigate the environmental risks posed by synthetic dyes in wastewater [1,2]. Adsorption is a type of mass transfer where different adsorbate species in aqueous systems are selectively adsorbed into the solid surface of the adsorbent. Although adsorption methods have demonstrated success in decolorizing textile discharges, their use is typically

*Corresponding author Tel.: +98 21 44787321
E-mail: bagheril@nigeb.ac.ir
DOI: 10.22104/AET.2024.6740.1840

restricted by the high cost of adsorbents [3-5]. Activated carbons, for example, have primarily been used to remove wastewater dye pollutants, but their cost is prohibitive [6,7]. As a result, many researchers have begun utilizing natural porous materials for pollutant adsorption (shown in Table 1).

Table 1. Comparing the highest adsorption capacities of different affordable sorbents for removing textile dye.

Adsorbent	Dye	Initial dye concentration (mg/l)	T (°C)	pH	mixing	Time (min)	q_{max} (mg/g)	References
Grinded and modified pumice	acid orange 7 direct yellow red 9	50	nd.	7	+	240	1.22 1.08	[8]
modified pumice	Methylene Blue	50	nd.	10	+	120	15.87	[5]
acidic treated pumice	Acid Red 14 Acid Red 18	100	nd.	3	+	180	3.1 29.7	[9]
Pumice powder	reactive azo dye	30	23°C	4	+	180	0.024	[10]
Pumice powder	Methylene Blue	50	nd.	4	+	60	0.362	[12]
Zeolite	Direct Yellow 50 (DY50)	40	30°C	3	nd.	240	83.33	[13]
Zeolite (Heulandite)	safranin dye	100	nd.	4	nd.	240	40	[14]
Zeolite (clinoptilolite)						240	37.2	
Zeolite (phillipsite)						480	30.26	
Raw scoria powder Iron-modified scoria	Malachite Green	85	nd.	11	nd.	75	2.4 3.6	[16]
Acidic treated scoria	Malachite Green	85	nd.	11	+	75	4.27	[17]
Pumice Scoria	direct black 22	50	22°C	4 5	+	120	7.71 8.1	[10]

These studies have highlighted the importance of using natural materials for adsorption purposes, prompting researchers to enhance their effectiveness through modifications. Pumice is indeed renowned for its highly porous structure and lightweight nature. It typically has a high silica content, often around 65%. These characteristics make it an excellent candidate for various applications, owing to its expansive surface area and exceptional adsorption capabilities. Gürses et al. [11] investigated the effectiveness of powdered pumice in eliminating Remazol Red RB. Their results showed that powdered pumice was a highly effective adsorbent for anionic dyes, with a high adsorption capacity. Moreover, powdered pumice utilized by Cifci and Meric demonstrated the highest level of adsorption capability of 0.362 mg/g for the removal of Methylene Blue from water solutions [12]. Subsequent modifications, as demonstrated by Derakhshan et al. [5], further enhanced pumice's efficacy, particularly in adsorbing cationic dyes, showing a significant increase in the capacity of adsorption. While pumice proves adept at removing both cationic and anionic dyes, its performance is generally more pronounced with cationic dyes. Ahmadian et al. [8] utilized ground and modified pumice to eliminate Acid Orange 7 and Direct Yellow Red 9, yielding the highest level of adsorption capability of 1.22 and 1.08 mg/g, respectively. Additionally, Samarghandi et al. [9] used acid-treated pumice for cationic dye Acid Red 14 removal, with the highest amount of adsorption capability of 3.1 mg/g. These combined results highlight the adaptability and promise of pumice as a potent adsorbent across diverse applications, particularly in dye removal. Among different natural adsorbents, zeolite stands out as a prominent candidate. Researchers have delved into its potential for dye removal applications. Alabbad [13] explored the efficacy of natural

zeolites in extracting Direct Yellow 50 (DY50) from dye solutions, revealing a notable maximum removal capacity of 83.33 mg/g. Additionally, Abukhadra and Mohamed [14] examined three separate classifications of natural zeolite, e.g., heulandite, clinoptilolite, and phillipsite, for safranin dye removal. Their findings showcased varying maximum adsorption capacities, with heulandite, clinoptilolite, and phillipsite demonstrating capacities of 40, 37.2, and 30.26 mg g^{-1}, respectively. Furthermore, efforts have been directed toward enhancing the surface properties of zeolite to enhance its adsorption capacity. For instance, Radoor and colleagues [15] investigated the ZSM-5 zeolite potential, modified with a biopolymer poly, to adsorb methylene blue from water. Their findings underscored the adaptability of the adsorption process, which could be tailored by adjusting operational variables like the quantity of zeolite utilized, initial dye concentration, contact time, temperature fluctuations, and pH levels. It is noteworthy that scoria, a naturally abundant material with a vast surface area, has emerged as a compelling option for adsorption purposes, particularly in water treatment applications. Due to its abundant presence on Earth and extensive surface area, it is a suitable adsorbent for purifying water sources by eliminating contaminants [16]. The effectiveness of scoria in removing malachite green from water has been extensively investigated. Studies have shown that under optimal conditions, such as a pH of 11, scoria exhibits the highest amount of adsorption capability of 3.6 mg/g over a duration of 75 minutes. Moreover, the effects of acid treatment on scoria, as explored by Sharafi et al. [17], have been found to significantly enhance its dye removal efficiency by increasing its surface area. Furthermore, Dugasa investigated the effectiveness of both pumice and scoria in eliminating direct black 22 from dye solutions and wastewater. Remarkably, after a 120-minute incubation period, pumice demonstrated a dye concentration reduction from 50 to 2.45 mg/l, while scoria exhibited a decrease to 3.1 mg/l [18]. These findings underscore the efficacy of scoria and its modified versions as valuable adsorbents in the dye removal process, highlighting their potential in water treatment and environmental remediation efforts. Moreover, silica, as a natural adsorbent, has been the subject of much research. Parida and colleagues [19]examined the process by which organic compounds were adsorbed onto the surface of silica samples. The presence of hydroxy groups and silanols on the silica surface was revealed using infrared spectroscopy, indicating surface negative charges on silica that had an affinity to adsorb the species lacking electrons. The pi-cloud was found to be involved in the hydrogen bond formation with the hydroxyl of silanol groups while aromatic compounds were being adsorbed. Hydrogen bonds occurred during the surfactant molecule adsorption on the silica surface. In addition, hydrogen bonds enabled silica surfaces to adsorb the surfactant compounds. The surfactants' polar moiety might also contribute to adsorption. Flat-on binding occurred between the styryl pyridinium dyes and the surface of the silica. Synthetic polymers adhered to the silica surface due to interactions between the multifunctional groups of the polymers and silanol groups. Furthermore, the Stober technique was employed to synthesize mesoporous silica nanoparticles (MSNs), which were subsequently modified with cysteine (MSN-Cys) to facilitate the removal of Methylene Blue (MB) from an aqueous solution. As the concentration increased, the MB adsorption rate also rose, which peaked at 140 mg of MB per gram of MSN-Cys. This was due to the physical interaction between Methylene Blue (MB) and the negative charge existing on the surface of the MSNs [20]. Until now, there has been a limited scope in comprehensive studies investigating the use of silicate stones in the adsorption process. In this research, the ability of SiO_2-based stone samples, including silica, zeolite, pumice, and scoria, to adsorb anionic and cationic dyes was examined. These porous stones, found abundantly in the natural environs of Iran, were examined for the adsorption of carmoisine and malachite green. Physicochemical properties were evaluated by analytical methods including FTIR, DLS, XRF spectroscopy, XRD, and BET. The isotherm and kinetic adsorption models were evaluated during dye adsorption by physically nano-sized stones.

2. Materials and methods

2.1. Chemicals

The experiment utilized exceptional-purity chemicals obtained from Merck Co., Germany. The Vista Zar Co. (http://www.vistazar.com/), which imports ROHA Company's IDACOL colors, supplied the carmoisine azo dye in commercial grade. The analytical-grade malachite green was acquired from Sigma Aldrich, and no additional purification was necessary.

2.2. Adsorbents: preparations and properties

Silica, zeolite, pumice, and scoria were obtained from local mines in Iran. The granular adsorbents were first mechanically pulverized using a Pneumatic Ring Mill (Daneshfanavaran Co., Iran), where the rotation speed of the blade was set at 250 rpm for four minutes. The powders were then transferred to a planetary ball mill (Retsch PM 100, Germany) to further refine the particles into a nano-sized scale. This type of ball milling is commonly used for its ability to alter the properties of rocks and create materials at the nanoscale [21]. The milling jar, containing eight ceramic balls, was tightly sealed, and the mill was operated at 450 rpm under normal conditions (25 ± 1°C). Ball milling was carried out in two 5-hour intervals for a total of 10-hours, with a 1-hour rest period between intervals. The effective diameters of the particles were estimated in a colloidal suspension solution (0.025 w/w %) through a dynamic light scattering (DLS) method [22] on a nanoparticle analyzer (ZetaPlus, Brookhaven) at a 90° scattering angle and a 25.2°C temperature. The surface area evaluation and pore volume of the adsorbent were conducted using the BET isotherm model. This evaluation was conducted via the nitrogen adsorption method, utilizing the gas's boiling point [23] using the BELSORP-mini II (BEL Japan Inc., Japan). In order to observe differences in wave number patterns related to the functional groups within the 400–4,000 cm^{-1} wavelength range, FTIR was used [24-25] (Nexus-870, Germany). The chemical compositions of the adsorbents were analyzed using X-ray fluorescence spectroscopy (Philips PW 1480, Netherlands). Additionally, in order to analyze XRD data to determine the crystalline structures of the adsorbents, a Philips diffractometer was utilized (Philips PW 3830, Netherlands) using CuKα radiation (λ=1.54 Å) [26-27].

2.3. Various adsorbents in dye adsorption experiments

The experiments explored dye adsorption by silica, zeolite, pumice, and scoria in both granular and nanoparticulate states. In each scenario, 10 mL of autoclaved, sterilized solution containing either carmoisine or malachite green dye at a concentration of 45 mg/L and a pH of 7 was statically incubated at 30°C. Subsequently, 2 g of a sterilized specific adsorbent type was added to each solution. Samples at prescribed times were centrifuged (13000 rpm, 5 min) to remove the particles. The supernatant was used to measure dye concentration using the spectrophotometry approach via the Epoch2 Microplate Reader (Bio Tek Company, USA). Intensities were recorded at maximum absorption wavelengths of carmoisine (λ_{max}= 515 nm) and malachite green (λ_{max}= 618 nm), respectively, for samples during carmoisine and MG removal processes. Intensities were converted to concentrations using a calibration curve for each dye.

2.4. Equilibrium dye adsorption

The correlation between dye concentration in solution and adsorbed dye specific mass under equilibrium at a constant temperature was investigated. For this purpose, nano-sized silica and/or scoria were assessed, respectively, for their adsorption capacity of carmoisine and malachite green at different concentrations (10, 20, 30, 40, and 50 mg/l). Equation 1 was employed to determine the equilibrium adsorption, q_e (mg/g), for the dataset once the system reached equilibrium.

$$q_e = \frac{V(C_0 - C_e)}{W} \quad (1)$$

The parameters C_0 (mg/l) and C_e (mg/l) signify the initial and equilibrium dye concentrations, respectively. V (l) indicates t the volume of solution, while w (g) denotes the adsorbent mass [5].

2.5. Adsorption isotherms

The equilibrium data was analyzed using two different equations for isotherms to determine the parameters of the adsorption isotherm.

2.5.1. Langmuir isotherm

The Langmuir adsorption model postulates uniformity among all adsorption sites, where the adsorption process at active sites remains uninfluenced by the presence or absence of molecules at nearby sites [28]. The Langmuir isotherm is used to evaluate the highest possible uptake from the covered monolayer of the adsorbent surface and is presented in a linearized form by Equation 2:

$$\frac{C_e}{q_e} = \frac{1}{K_L} + \frac{a_L}{K_L} C_e \quad (2)$$

where C_e (mg/l) is the concentration of unabsorbed dye in the solution, q_e (mg/g) indicates the quantity of dye adsorbed per unit weight of adsorbent [28-29], K_L (l/g) stands for the Langmuir equilibrium constant, and the K_L/a_L ratio signifies the theoretical maximum adsorption capability at monolayer saturation, expressed as q_m (mg/g) [28]. The separation factor, also known as the equilibrium parameter (R_L), summarizes the main features of the Langmuir isotherm into a dimensionless constant and is denoted by Equation 3:

$$R_L = \frac{1}{1 + a_L C_0} \quad (3)$$

where C_0 and a_L (l/mg) represent the initial dye concentration and w the Langmuir constant reflecting the adsorption energy, respectively[15,30,31]. The R_L value serves as an indicator: values higher than 1 suggest an undesirable isotherm profile, 1 indicates linearity, values between 0 and 1 show desirability, and 0 suggests irreversibility [15,17,30-32].

2.5.2. Freundlich isotherm

The Freundlich isotherm is formulated to describe multilayer adsorption that occurs on surfaces with varying properties [30]. Equation 4 represents this empirical isotherm:

$$\ln q_e = \ln K_f + \frac{1}{n} \ln C_e \quad (4)$$

where K_f represents the Freundlich constant ((mg/g) $(l/mg)^{1/n}$), associated with the sorption capacity (mg/g), while n represents an empirical value indicative of the sorption intensity [30]. The non-dimensional heterogeneity factor "*n*" shows the equilibrium interaction between the adsorbent and adsorbate, where values between 1 and 10 signify favorable adsorption. A value less than 1 for *1/n* suggests a robust interaction between the adsorbent and adsorbate, while a value close to 1 suggests uniform adsorption energy across all active sites of the adsorbent [31-32].

2.6. Adsorption kinetics

To understand the kinetics of dye adsorption, various kinetic equations such as the pseudo-first-order, pseudo-second-order, intra-particle diffusion, and Elovich models were employed for characterization [5].

2.6.1. Pseudo-first-order kinetics

The pseudo-first-order model suggests that the solute adsorption rate depends on the maximum adsorption capacity [29]. Equation 5 provides the linear behavior of the pseudo-first-order model:

$$-k_1 t = \ln(q_e - q_t) - \ln q_e \quad (5)$$

where k_1 represents the rate constant for pseudo-first-order adsorption (min^{-1}), while q_e (mg/g) and q_t (mg/g) denote the dye adsorbed amount per unit mass of adsorbent at equilibrium and at time t, respectively [33].

2.6.2. Pseudo second-order kinetics

In the pseudo-second-order model, the step that limits the rate involves the formation of a chemisorptive bond between the adsorbate and the adsorbent, which entails electron sharing or exchange [28]. Equation 6 represents this kinetic model of the pseudo-second-order:

$$\frac{1}{k_2 {q_e}^2} + \frac{t}{q_e} = \frac{t}{q_t} \quad (6)$$

where k_2 represents the rate constant for pseudo-second-order adsorption (g mg^{-1} min^{-1}) [34].

2.6.3. Intraparticle diffusion kinetics

The linear relationship observed when plotting the mass ratio of dye to the adsorbent against the square root of the contact time shows that

intraparticle diffusion governs the rate-limiting step in the process of dye adsorption. This relationship is described by Equation 7, which represents the equation of intraparticle diffusion.

$$q_t = k_p t^{1/2} \quad (7)$$

where k_p denotes the intraparticle diffusion rate constant (mg g^{-1} $min^{-1/2}$) [35]. Moreover, R_i can be computed as the ratio between the initially adsorbed mass (q_0) and the ultimately adsorbed mass (q_e), according to Equation 8.

$$R_i = 1 - \frac{q_0}{q_e} \quad (8)$$

R_i can be classified into one of four categories: weak initial adsorption (Zone I) occurs when $0.9 < R_i < 1$; intermediate initial adsorption (Zone II) occurs when $0.5 < R_i < 0.9$; strong initial adsorption (Zone III) occurs when $0.1 < R_i < 0.5$; and complete initial adsorption occurs when $0.1 > R_i$ (Zone IV) [35].

2.6.4. Elovich kinetics

The Elovich equation (Equation 9) [36] is another kinetic model used to analyze transient data.

$$q_t = \frac{1}{\beta}\ln(\alpha\beta) + \frac{1}{\beta}\ln t \quad (9)$$

where α (mg g^{-1} min^{-1}) and β (g/mg) represent the rate constant of initial sorption and correlates with the level of surface saturation and the energy needed for chemisorption, respectively [36].
The dimensionless Elovich equation is outlined in Equation 10:

$$\frac{q_t}{q_e} = R_E \ln\left(\frac{t}{t_e}\right) + 1 \quad (10)$$

where t_e is the lengthiest adsorption time and q_e is solid phase concentration at time t_e. $R_E = \frac{1}{\beta \times q_e}$ approaches the equilibrium factor of the Elovich equation, which affects the curvature of the curves of q_t/q_e versus t/t_e [37]. These curves may appear flat or sloping depending on curvature, which is influenced by R_E values. Four ranges can be distinguished. When R_E is greater than 0.3 (Zone I), the curve exhibits a gradual increase; when R_E falls between 0.1 and 0.3 (Zone II), the curve shows a moderate rise. When R_E ranges from 0.02 to 0.1 (Zone III), the curve demonstrates a rapid ascent; when R_E is below 0.02 (Zone IV), the curve quickly approaches equilibrium [37]. The Elovich equation effectively characterized the kinetic behavior of numerous adsorption systems with a gentle rising trend [37].

3. Results and discussion

3.1. Physico-chemical properties of adsorbents

The average dimensions of pulverized silica, zeolite, pumice, and scoria calculated using dynamic light scattering were found to be 278 nm, 227 nm, 147 nm, and 262 nm, respectively. This indicated that ball milling could successfully produce nanoparticles from these materials. According to Zhang et al. [38], ball milling for 12 hours yielded chitosan particles ranging in diameter from 360 to 375 nm. Jeong et al. [39] found that aggregated Y_2O_3 nanoparticles were efficiently crushed by ball milling into particle sizes of 34 nm. Saepurahman and Hashaikeh reported that micro H-Y zeolites underwent high-energy ball milling for 30 minutes, resulting in the production of nanoparticles ranging from 50 to 100 nm [40]. BET studies were generated to estimate the overall pore volume and surface area of each specimen, with the findings presented in Table 2. The results demonstrate that all the nanosized samples had greater specific area and total pore volume than their granular counterparts, which might contribute to enhanced adsorption. Consequently, nanosized samples adsorbed anionic and cationic dyes more rapidly than their granular counterparts [41]. The XRD profiles of different samples were also acquired for this study, as depicted in Figure 1. Using JCPDS file number 33-1161, the XRD data (Figure 1) identified quartz as the dominant phase in the silica sample. According to Zemnukhova et al. [42], an XRD analysis of the silica sample showed a single broad peak at approximately $2\theta \approx 22°$, characteristic of amorphous structures. Furthermore, Samadi-Maybodi and Atashbozorg [43] showed that the XRD spectrum of pure silica showed a significant peak within the range of $2\theta \approx 18–30°$, assigned to an amorphous structure. The XRD pattern shown in Figure 1 helped identify the principal phases in the zeolite sample as clinoptilolite (JCPDS file no. 39-1383), quartz (JCPDS file no. 33-1161), and cristobalite (JCPDS file no. 39-1425). According to the findings of Mansouri et al. [44], the XRD pattern for a zeolite sample revealed intense diffractions that might be

assigned to clinoptilolite. Castaldi et al. [45,46] also observedthat the activated zeolite predominantly included clinoptilolite. The XRD analysis of the pumice sample was identified predominantly as amorphous, anorthite (JCPDS file no. 18-1202), and hornblende (JCPDS file no. 45-1371) (Figure 1). Previously, Safari et al. found that there was a broad peak between 2θ ≈ 20–40° on the XRD spectrum of pumice samples, indicating the presence of an amorphous phase [47]. Guler and Sarioglu [33] identified 2θ≈ 26.65° in the XRD pattern of pumice stone, indicating the presence of an amorphous quartz material. The XRD data shown in Figure 1 revealed that the primary phases for the scoria sample were augite (according to JCPDS file no. 24-0203), mica–illite (JCPDS file no. 26-0911), and amorphous. Depci et al. [48] previously reported that scoria was mostly amorphous, although certain crystalline mineral phases, such as anorthite, hornblende, and crystalline quartz, were observed in the XRD pattern.

Furthermore, the elemental composition of the stones was assessed using XRF analysis. The XRF data in Table 3 demonstrated that SiO_2 was the most abundant component of all the studied samples. The silica, zeolite, pumice, and scoria samples correspondingly comprised ~99%, ~70%, ~66%, and ~50% SiO_2, respectively. Mansouri et al. [44] revealed that SiO_2 (68.17%), Al_2O_3 (11.05%), and CaO (1.11%) are the major constituents in their zeolite sample. In addition, Safari et al. [35] showed that the primary chemical constituents of a pumice sample were SiO_2 (63.45%) and Al_2O_3 (17.24%). Chemical analysis by Depci et al. [48] also found that SiO_2 (54.92%), Al_2O_3 (16.92%), Fe_2O_3 (10.31%), and CaO (6.47%) represented the principal constituents of a scoria sample. Moreover, FTIR analysis was used to determine the main functional groups in the stone samples. In the FTIR spectra (Figure 2), a peak around 790 cm^{-1} was attributed to the bending vibrations of Si–O bonds in the amorphous quartz. Symmetric vibrations in the range of 1020–1095 cm^{-1} were related to Si-O-Al bonds. The peak at 3400 cm^{-1} indicated OH stretching vibrations, characteristic of water. A band near 1600 cm^{-1} was attributed to the bending vibration of OH groups corresponding to adsorbed water [47-50].

Table 2. Surface area and overall pore volume determined through BET analysis for the samples.

Sample	Specific surface area (m^2/g)	Total pore volume (cm^3/g)
Granular Silica	1.11	0.0013
nano-sized Silica	2.65	0.0155
Granular Zeolite	12.78	0.0891
nano-sized Zeolite	22.15	0.2013
Granular Pumice	2.85	0.0275
nano-sized Pumice	5.36	0.0324
Granular Scoria	0.81	0.0023
nano-sized Scoria	2.36	0.01436

Table 3. Chemical composition of samples measured by XRF analysis.

Component	Silica % (w/w)	Zeolite % (w/w)	Pumice % (w/w)	Scoria % (w/w)
SiO_2	99.32	69.80	65.77	49.76
Al_2O_3	0.01	10.42	15.99	13.13
Fe_2O_3	0.20	0.41	2.21	5.22
CaO	0.10	0.55	3.95	13.12
Na_2O	0.01	2.47	2.07	3.56
K_2O	0.01	4.87	2.62	3.78
MgO	0.01	0.15	0.84	6.63
TiO_2	0.043	0.212	0.416	1.446
MnO	0.008	0.007	0.048	0.098
P_2O_5	0.001	0.007	0.177	1.578
L.O.I	0.16	10.74	5.44	0.47
SO_3	0.02	0.15	0.03	0.45

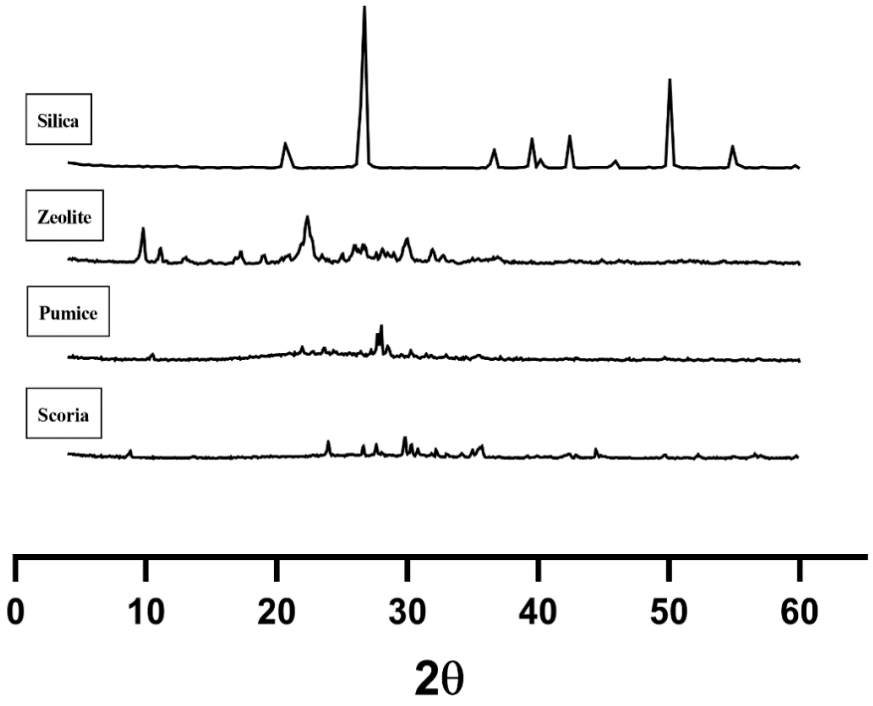

Fig. 1. XRD profiles for natural silica, zeolite, pumice, and scoria.

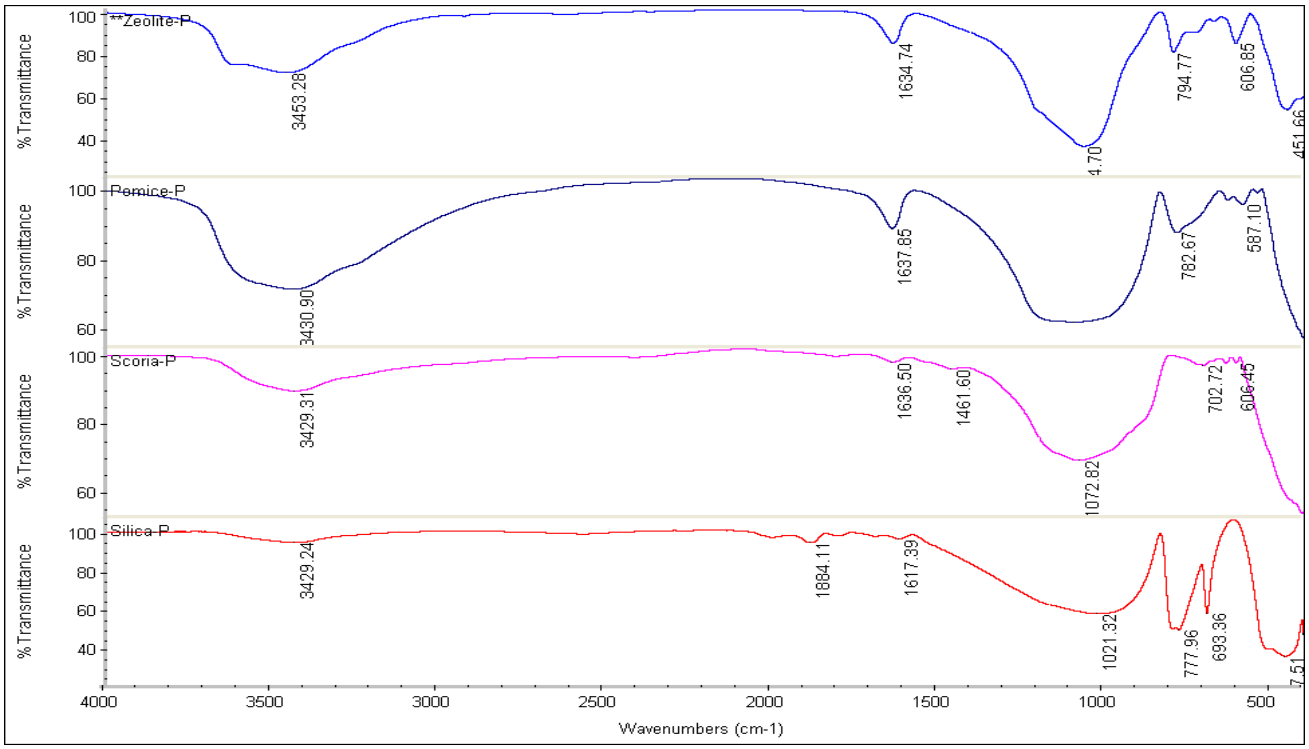

Fig. 2. FTIR patterns for powdered silica, scoria, pumice, and zeolite.

3.2. Dye adsorption

This research investigated the adsorption of carmoisine or malachite green from water using both granular and nano-sized stones, with an initial dye concentration of 45 mg/l. Figure 3a shows that the absence of an adsorbent in the control experiments resulted in insignificant changes in dye concentrations. Granular

adsorbents exhibited minimal dye removal (Figure 3a), whereas nano-sized stones demonstrated greater efficiency in dye removal (Figure 3b) due to their extensive specific surface area and pore volume, as determined through BET analysis. Nano-sized silica completely adsorbed carmoisine during 15 days of incubation (Figure 3b). And even though granular adsorbents could remove a significant amount of malachite green over a period of several days (Table 4), nano-sized adsorbents could accomplish removal in a matter of hours (Table 4). After only two hours, nano-sized scoria was able to remove the malachite green (45 mg/l) completely.

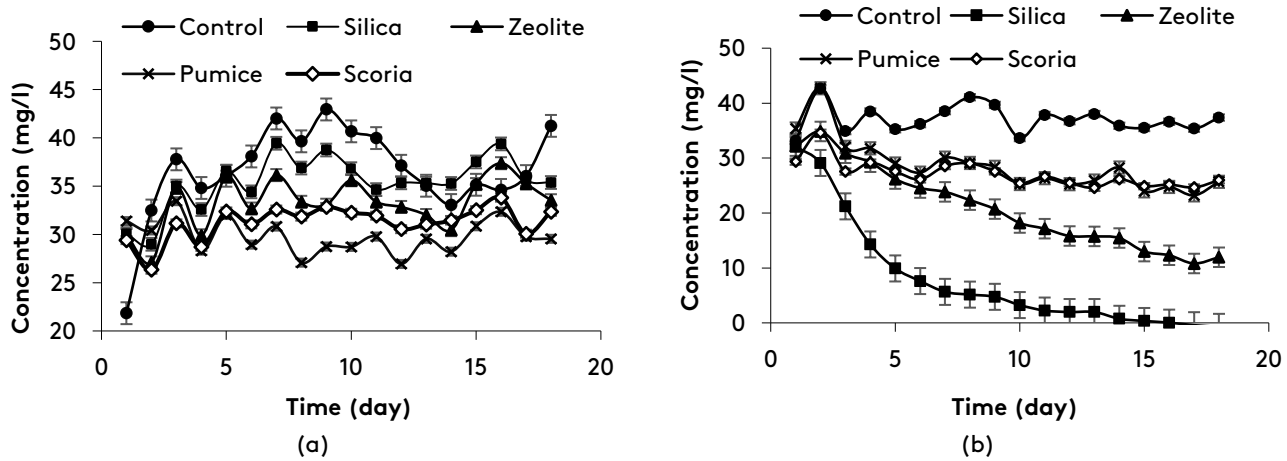

Fig. 3. Carmoisine adsorption by (a) granular and (b) nano-sized stones performed at 30°C and pH 7 under static conditions with 45 mg/l initial dye concentration.

The anionic azo dye, carmoisine, becomes charged negatively when solubilized in water at the normal pH (6 to 8) [51-53]. Because of the negative surface charge of SiO_2 [54-56], carmoisine is expected to be electrostatically repelled by silica-based stones. Yet, carmoisine adsorption was found to be enhanced with increased SiO_2 content (Figure 3b), and the silica sample with the highest content of SiO_2 (Table 3) showed the greatest amount of dye adsorption. These observations may be supported by Scott's explanation of the multilayer adsorption process of water on silica, which shows hydroxyl groups binding to silanol on silica [57]. In this study, a polar solvent interacted with the silica surface by forming hydrogen bonds with water molecules present on the surface. Accordingly, it could be hypothesized that a hydrogen bond between the carmoisine functional groups and surface water molecules on the silica-based stones was responsible for dye adsorption. Thus, the association between higher silica levels and higher dye adsorption was substantiated. Malachite green, a cationic dye, carries a positive charge in water [58-59]; it is expected to be electrostatically adsorbed on silica-based stones due to the negative surface charge of SiO_2. However, our observations (Table 4) indicated that malachite green adsorption decreased with increasing SiO_2 content and that scoria, with the lowest content of SiO_2 (Table 3), exhibited the highest dye adsorption. The limitation for malachite green electrostatic adsorption on SiO_2-based stones is believed to arise from steric hindrance due to hydrogen interactions between malachite green functional groups and surface water molecules.

3.3. Equilibrium studies

The Langmuir and Freundlich models were used to examine the correlation between equilibrium adsorption (q_e) and equilibrium dye concentration (c_e). Upon fitting the isotherm data using the Langmuir equation, the correlation coefficients (R^2) for carmoisine adsorption on nano-sized silica and malachite green adsorption on nano-sized scoria were determined to be 0.962 and 0.933, respectively, through linear regression analysis (Table 5). Moreover, the separation factor (R_L) for the adsorption of carmoisine on silica (0.087) and malachite green on scoria (0.083) decreased between 0 and 1, suggesting that the Langmuir model exhibited a favorable isotherm profile [31-

32]. Lower R_L values also indicated that adsorption was more favorable [31]. The Langmuir model used the formation of a single molecular layer on the surface of the adsorbent, indicating that each adsorption site accommodated only one dye molecule, and intermolecular forces decreased with distance. Additionally, the model assumed a homogeneous adsorbent surface with uniform and energetically similar adsorption sites [31].

Table 4. Duration of complete adsorption of malachite green with 45 mg/l initial concentration under static conditions at 30°C and pH 7.

Sample	Duration
Granular silica	13-days
nano-sized silica	8-hours
Granular zeolite	2-days
nano-sized zeolite	5-hours
Granular pumice	2-days
nano-sized pumice	4-hours
Granular scoria	3-days
nano-sized scoria	3-hours

After applying the Freundlich isotherm model to the carmoisine adsorption data on silica, the correlation coefficient (R^2) and the isotherm constant, *n*, were 0.961 and 0.912, respectively. The experimental adsorption data aligns well with the Freundlich model. Additionally, the calculated n value of 1.731 for carmoisine adsorption on silica falls within the desirable adsorption range of 1 to 10, suggesting strong interaction between the adsorbent and adsorbate with $1/n < 1$ [31-32]. The Freundlich isotherm model was formulated to explain adsorption mechanisms that entail multilayer adsorption and surfaces with varying properties. The utilization of both the Langmuir and Freundlich isotherm models in studying the adsorption of carmoisine onto silica nano-sized stones suggested that the adsorption phenomenon involved both monolayer formation and heterogeneous surfaces [33].

Table 5. Langmuir and Freundlich isotherm constants. * carmoisine adsorption on nanosized-silica, ** malachite green adsorption on nanosized-scoria.

Isotherm	Constants	carmoisine*	malachite Green**
Langmuir	**q_m (mg/g)**	0.300	0.028
	K_L (l/g)	0.069	0.007
	a_L (l/mg)	0.232	0.245
	R^2	0.962	0.933
	R_L	0.087	0.083
Freundlich	**n**	1.731	0.285
	K_f (mg/g) (l/mg)$^{1/n}$	0.061	0.069
	R^2	**0.961**	**0.912**

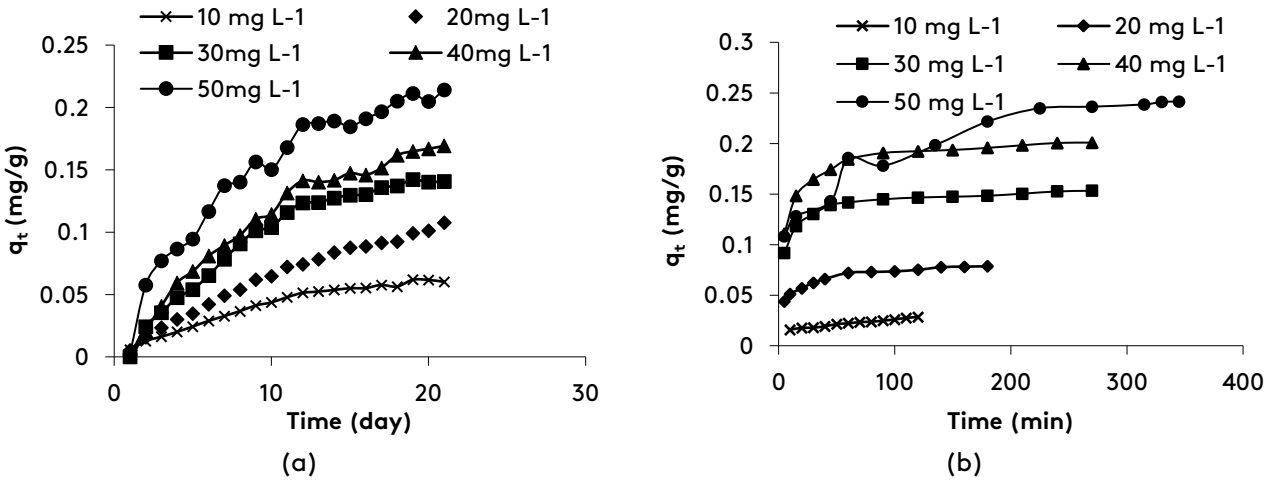

Fig. 4. Adsorption kinetics of (a) carmoisine on nano-sized silica, and (b) malachite green on nano-sized scoria at different initial dye concentrations.

3.4. Kinetic studies

Figure 4 demonstrates the impact of initial dye concentrations and contact time on the carmoisine adsorption and malachite green adsorption by nanosized silica and scoria, respectively. With increasing contact time, dye adsorption increased, and equilibrium was achieved during 12 days for carmoisine and two hours for malachite green. The duration to achieve equilibrium remained constant regardless of the initial dye concentration. Nonetheless, higher initial dye concentrations exhibited a faster initial adsorption rate. This phenomenon arose from the concentration's impact on the dye's diffusion to the adsorbent's surface in the absence of mixing. Increased dye concentration accelerated dye molecule diffusion from solution to adsorbent by enhancing the concentration gradient's driving force [60]. The key factors impacting the equilibrium capacity and rate were the surface area of the adsorbent, its physicochemical properties, the accessibility for adsorbate molecules or ions, and the size and shape of its particles [61-63].

Transport of mass or bulk in the aqueous phase and diffusivity into the aqueous layer around the adsorbents or pores are the dominant mechanisms that control the adsorption process [61-63]. Various kinetic models were employed to explore the governing of the adsorption process, encompassing diffusion control and mass transfer. Investigations into kinetics involved employing equations, such as pseudo-first-order, intraparticle diffusion, pseudo-second-order, and Elovich. Tables 6 and 7 present the estimated kinetic and correlation coefficients for carmoisine and malachite green adsorption, respectively. The rate constant k_1 for the first-order reaction and equilibrium adsorption density q_e were identified by analyzing the gradients and intercepts of $ln\ (q_e\text{-}q_t)$ versus t (Tables 6 and 7). Most of the correlation constants associated with the first-order kinetic model for all concentrations examined were below 0.966. Additionally, there was a significant disparity between the calculated value of $q_{e,cal}$ and the experimental value of $q_{e,exp}$. To investigate the pseudo-second-order equation, this study employed the gradients and intercepts obtained from plots of t/q_t against t to identify the pseudo-second-order rate constant k_2 and the equilibrium adsorption density q_e (Tables 6 and 7). The correlation coefficients associated with the second-order kinetic equation exceeded 0.966 across all concentrations except one. The computed $q_{e,cal}$ values from the pseudo-second-order equation also closely matched the data obtained through experimentation ($q_{e,exp}$), indicating that the second-order kinetic model might offer a more accurate depiction of the studied systems compared to the first kinetic equation. In the second-order kinetic process, the step that determines the overall rate is considered to involve electron sharing or exchange between the adsorbate and the adsorbent [28]. The pseudo-second-order equation relies on the solid phase adsorption potential and corresponds to the idea that the step controlling the rate involves a chemisorption mechanism.

Table 6. Comparison of rate constants of various kinetic equations and experimental and calculated q_e for various initial carmoisine concentrations.

		Pseudo-first-order equation			Pseudo-second-order equation			Intraparticle diffusion			Elovich equation			
C_0 (mg/l)	$q_{e,exp}$ (mg/g)	k_1 (min^{-1})	$q_{e,cal}$ (mg/g)	R^2	k_2 (g mg^{-1} min^{-1})	$q_{e,cal}$ (mg/g)	R^2	k_p (mg g^{-1} $min^{-1/2}$)	R_i	R^2	A (mg g^{-1} min^{-1})	B (g/mg)	R_E	R^2
10	0.055	0.111	0.325	0.905	1.142	0.091	0.966	0.014	1.007	0.973	0.022	52.083	0.210	0.951
20	0.099	0.067	0.391	0.971	0.402	0.174	0.952	0.024	1.475	0.980	0.035	30.303	0.189	0.938
30	0.127	0.124	0.485	0.891	0.447	0.220	0.970	0.035	1.034	0.973	0.050	21.551	0.210	0.960
40	0.1643	0.079	0.498	0.910	0.335	0.265	0.987	0.041	1.044	0.986	0.056	18.818	0.203	0.973
50	0.205	0.081	0.506	0.962	0.617	0.272	0.979	0.047	0.964	0.980	0.010	17.094	0.214	0.959

Table 7. Comparison of rate constants of various kinetic equations, and experimental and calculated q_e for various initial malachite green concentrations.

		Pseudo-first-order equation			Pseudo-second-order equation			Intraparticle diffusion			Elovich equation			
C_0 (mg l^{-1})	$q_{e,exp}$ (mg g^{-1})	k_1 (min^{-1})	$q_{e,cal}$ (mg g^{-1})	R^2	k_2 (g mg^{-1} min^{-1})	$q_{e,cal}$ (mg g^{-1})	R^2	k_p (mg g^{-1} $min^{-1/2}$)	R_i	R^2	A (mg g^{-1} min^{-1})	B (g mg^{-1})	R_E	R^2
10	0.028	0.095	0.182	0.865	1.63	0.031	0.977	0.001	0.654	0.977	0.007	196.078	0.182	0.906
20	0.073	0.276	0.3508	0.893	1.591	0.081	0.999	0.002	0.403	0.907	0.174	101.010	0.135	0.988
30	0.146	0.291	0.3872	0.991	1.172	0.154	0.999	0.003	0.275	0.744	3.638	70.921	0.100	0.928
40	0.192	0.305	0.4999	0.937	0.728	0.204	0.999	0.005	0.932	0.779	1.294	46.728	0.112	0.950
50	0.234	0.146	0.512	0.875	0.156	0.256	0.999	0.008	0.574	0.950	0.099	28.818	0.150	0.943

Adsorption versus time plots at different initial dye concentrations were used to assess the contribution of diffusion to adsorption [28]. The graph of q_t against $t^{1/2}$ showed a linear connection (Figure 5), suggesting that intraparticle diffusion kinetics contributed to the removal of carmoisine and malachite green. According to Tables 6 and 7 and the Wu et al. classification [35], the overall R_i values for the carmoisine adsorption process indicated weak initial adsorption. The R_i values for malachite green adsorption suggested that initial adsorption occurred within the intermediate zone. Although the Elovich equation does not specify a particular process, it proves valuable in comprehending adsorption on extremely heterogeneous adsorbents [61]. The Elovich kinetic constants of α and β (given in Tables 6 and 7) originated from the gradients of graphs depicting q_t against *ln (t)* (Figure 6). The coefficients of correlation provided in Tables 6 and 7 for the Elovich equation exhibited a decrease compared to those of the pseudo-second-order equation. These tables present the kinetic parameters pertaining to carmoisine and malachite green adsorptions. Based on the Wu et al. classifications [37], with R_E = 0.1 and 0.3 representing a slight rise at the curves, the kinetic mechanism might not be adequately substantiated by the Elovich equation.

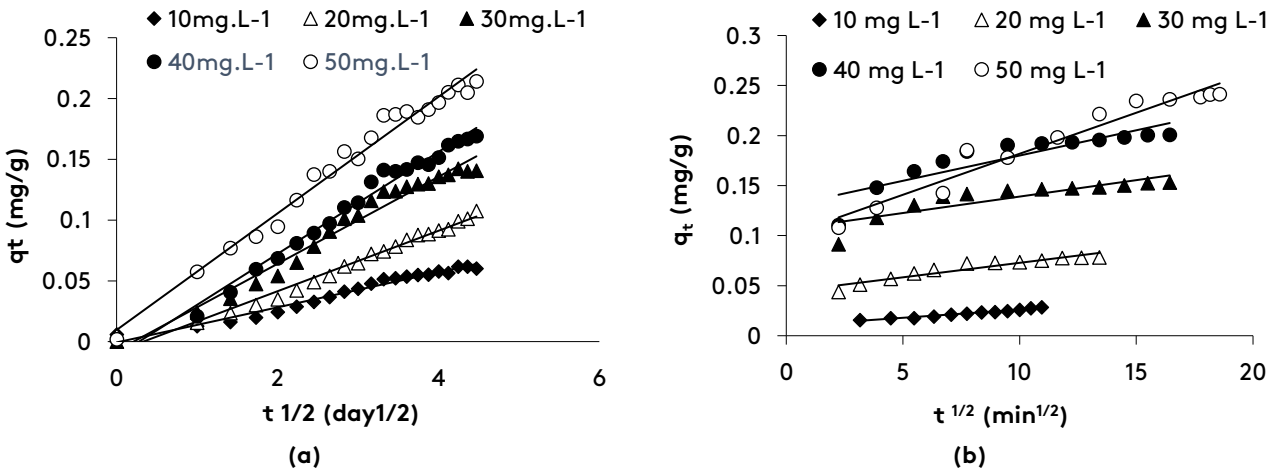

Fig. 5. Graphs representing the intraparticle diffusion equation for the adsorption of (a) carmoisine on nano-sized silica and (b) malachite green on nano-sized scoria at different initial concentrations.

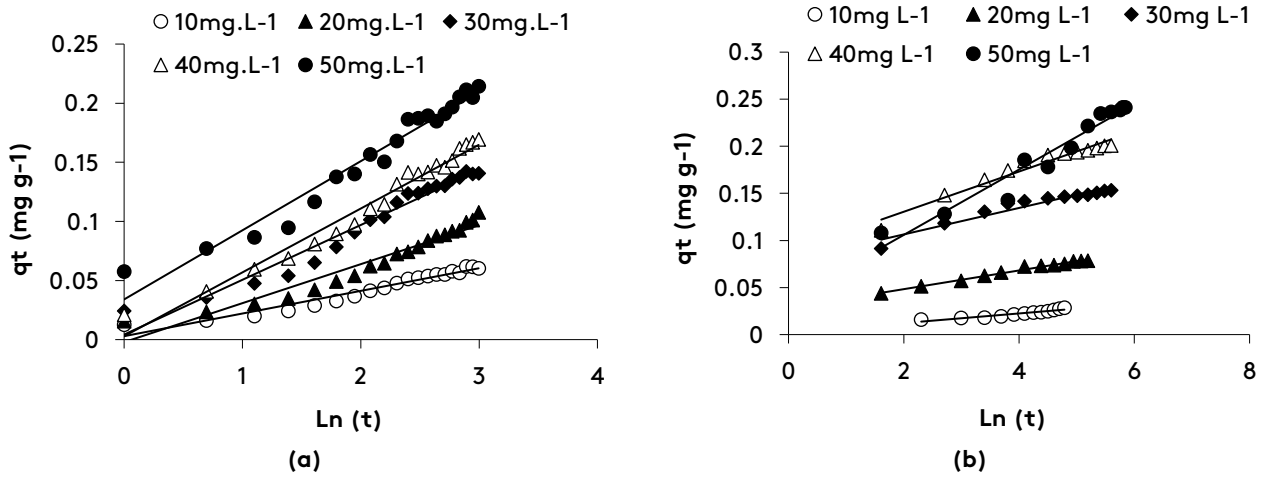

Fig. 6. Figures of the Elovich equation for the adsorption of (a) carmoisine on nano-sized silica and (b) malachite green on nano-sized scoria at different initial concentrations. T is the time in days for the graph (a) and minutes for the graph (b).

4. Conclusions

The objective of this investigation was to evaluate the adsorption characteristics of silicate minerals in eliminating both anionic and cationic dyes. The results revealed the influence of silicate percent on the adsorption processes. Nanosized silica and nanosized scoria demonstrated considerable efficacy in removing both cationic and anionic dyes from water. Specifically, the adsorption of carmoisine dye exhibited an upward trend with increasing SiO_2 percentage. Remarkably, the silica sample exhibiting the greatest SiO_2 content demonstrated the most substantial capacity for dye adsorption. The involvement of multilayer water adsorption on silica, leading to the binding of hydroxyl groups to silanol sites, was identified as a crucial factor in dye adsorption. Conversely, malachite green dye adsorption decreased with an increase in SiO_2. Interestingly, the scoria with the lowest SiO_2 percent demonstrated the highest dye adsorption among the samples. Studies were also conducted on the equilibrium and kinetics of dye adsorption into nanosized adsorbents. The Langmuir isotherm model exhibited superior applicability to carmoisine adsorption onto nanosized silica and malachite green adsorption onto nanosized scoria. In the examined dye adsorption systems, the pseudo-second-order equation showed the best alignment with the experimental results. This equation relies on the adsorption capacity of the solid phase, aligning with a chemisorption mechanism as the rate-

controlling step. In further academic exploration, the impacts of factors such as pH, temperature, and cross-sectional properties on the adsorption mechanism can be investigated.

Acknowledgements

The author wishes to extend sincere appreciation to the National Institute of Genetic Engineering and Biotechnology (NIGEB) for their invaluable support, which significantly contributed to the successful conclusion of this study endeavor.

References

[1] Sharafinia, S., Farrokhnia, A. and Lemraski, E.G., (2022). The adsorption of cationic dye onto ACPMG@ZIF-8 core-shell, optimization using central composite response surface methodology (CCRSM). *Colloids and surfaces A: physicochemical and engineering aspects, 634*, 128039. https://doi.org/10.1016/j.colsurfa.2021.128039

[2] Salman, N. S., Alshamsi, H. A. (2022). Synthesis of sulfonated polystyrene-based porous activated carbon for organic dyes removal from aqueous solutions. *Journal of polymers and the environment*, *30*(12), 5100-5118. https://doi.org/10.1007/s10924-022-02584-1

[3] Asefa, M. T., Lelisa, W., Feyisa, G. B. (2022). Comparative study on removal efficiency of methylene blue from wastewater by using nano-scaled sugarcane bagasse ash and jema silica sand. *International of journal of water wastewater treat*, *8*(1). https://doi.org/10.16966/2381-5299.181

[4] Xia, K., Liu, X., Chen, Z., Fang, L., Du, H. and Zhang, X. (2020). Efficient and sustainable treatment of anionic dye wastewaters using porous cationic diatomite. Journal of the Taiwan Institute of Chemical Engineers, 113, 8-15. DOI: 10.1016/j.jtice.2020.07.020

[5] Derakhshan, Z., Baghapour, M., A., Ranjbar, M., Faramarzian, M. (2013). Adsorption of methylene blue dye from aqueous solutions by modified pumice stone: Kinetics and equilibrium studies, *Health scope*. *2*, 136–144. https://doi.org/10.17795/jhealthscope-12492

[6] Salman, N.S. and Alshamsi, H.A. (2022). Synthesis of sulfonated polystyrene-based porous activated carbon for organic dyes removal from aqueous solutions. *Journal of polymers and the environment, 30*, 5100-5118. DOI:10.21203/rs.3.rs-1754062/v1

[7] Joshua, O. I., Adewale G. A., Omodele A. A. E., Lois T. A. (2021). Competitive adsorption of Pb(II), Cu(II), Fe(II) and Zn(II) from aqueous media using biochar from oil palm (Elaeis guineensis) fibers: a kinetic and equilibrium study, *Indian chemical engineer, 63*(5), 501-511. DOI: 10.1080/00194506.2020.1787870.

[8] Ahmadian, M., Yosefi, N., Toolabi, A., Khanjani, N., Rahimi, S., Fatehizadeh, A. (2012). Adsorption of direct yellow 9 and acid orange 7 from aqueous solutions by modified pumice. *Asian journal of chemistry*, *24*(7), 3094. http://irdoi.ir/320-725-667-161.

[9] Samarghandi, M. R., Zarrabi, M., Sepehr, M. N., Amrane, A., Safari, G. H., Bashiri, S. (2012). Application of acidic treated pumice as an adsorbent for the removal of azo dye from aqueous solutions: kinetic, equilibrium and thermodynamic studies. *Iranian journal of environmental health science and engineering*, *9*, 1-10. https://doi.org/10.1186/1735-2746-9-9.

[10] Veliev, E. V., Öztürk, T., Veli, S., Fatullayev, A. G. (2006). Application of diffusion model for adsorption of azo reactive dye on pumice. *Polish Journal of environmental studies*, *15*(2)., 347–353.

[11] Gürses, A., Güneş, K., Şahin, E. and Açıkyıldız, M. (2023). Investigation of the removal kinetics, thermodynamics and adsorption mechanism of anionic textile dye, Remazol Red RB, with powder pumice, a sustainable adsorbent from waste water. *Frontiers in chemistry, 11*, 1156577. https://doi.org/10.3389/fchem.2023.1156577.

[12] Çifçi, D. İ., Meric, S. (2016). Optimization of methylene blue adsorption by pumice powder. *Advances in environmental research*, *5*(1), 37-50. https://doi.org/10.12989/AER.2016.5.1.037.

[13] Alabbad, E. A. (2021). Efficacy assessment of natural zeolite containing wastewater on the adsorption behaviour of Direct Yellow 50 from; equilibrium, kinetics and thermodynamic

studies. *Arabian journal of chemistry*, *14*(4), 103041. https://doi.org/10.1016/j.arabjc.2021.103041

[14] Abukhadra, M. R., Mohamed, A. S. (2019). Adsorption removal of safranin dye Contaminants from Water using Various types of natural zeolite, *Silicon*. *11*, 1635–1647. https://doi.org/10.1007/s12633-018-9980-3.

[15] Radoor, S., Karayil, J., Jayakumar, A., Parameswaranpillai, J., Siengchin, S. (2021). Removal of methylene blue dye from aqueous solution using PDADMAC modified ZSM-5 zeolite as a novel adsorbent. *Journal of polymers and the environment, 29*, 3185-3198.

[16] Osouleddini N., Moradi, M., Khosravi, T., Khamotian, R., Sharafj, H. (2018). The iron modification effect on performance of natural adsorbent scoria for malachite green dye removal from aquatic environments: modeling, optimization, isotherms, and kinetic evaluation, *Desalination water treat*. *123*, 348–357. https://doi.org/10.5004/dwt.2018.22658

[17] Sharafi, K., Dargahi, A., Azizi, N., Amini, J., Ghayebzadeh, M., Rezai, Z., Moradi, M. (2018). Investigating the effect of Nitric acid (with different normalities) on the efficiency of scoria in Malachite removal from aquatic environments: determination of model, isotherms and reaction kinetics, *Journal of*. *Environmental*. *Science and*. *Technol*. *20*, 45–62. https://doi.org/10.22034/jest.2018.13255

[18] Dugasa A., Eba K., Endale H., (2018). Adsorptive removal of direct black 22 dye using pumice and scoria from aqueous solution and wastewater, Institute of health sciences, https://repository.ju.edu.et/handle/123456789/2240.

[19] Parida, S. K., Dash, S., Patel, S., Mishra, B. K. (2006). Adsorption of organic molecules on silica surface. *Advances in colloid and interface science*, *121*(1-3), 77-110. https://doi.org/10.1016/j.cis.2006.05.028.

[20] Beagan, A.M. (2021). Investigating methylene blue removal from aqueous solution by cysteine-functionalized mesoporous silica. *Journal of chemistry, 1*-12. https://doi.org/10.1155/2021/8839864.

[21] Rigopoulos, I., Török, Á., Kyratsi, T., Delimitis, A., Ioannou, I. (2018). Sustainable exploitation of mafic rock quarry waste for carbon sequestration following ball milling. Resources Policy, 59, 24-32.

[22] Hoo, C.M., Starostin, N., West, P. and Mecartney, M.L. (2008). A comparison of atomic force microscopy (AFM) and dynamic light scattering (DLS) methods to characterize nanoparticle size distributions. *Journal of nanoparticle research, 10,* 89-96.

[23] Ambroz, F., Macdonald, T.J., Martis, V. and Parkin, I.P. (2018). Evaluation of the BET Theory for the Characterization of Meso and Microporous MOFs. *Small methods, 2*, 1800173. https://doi.org/10.1002/smtd.201800173

[24] Perez-Calderon, J., Marin-Silva, D.A., Zaritzky, N. and Pinotti, A. (2023). Eco-friendly PVA-chitosan adsorbent films for the removal of azo dye Acid Orange 7: Physical cross-linking, adsorption process, and reuse of the material. *Advanced industrial and engineering polymer research, 6*, 239-254. https://doi.org/10.1016/j.aiepr.2022.12.001

[25] Paredes-Laverde, M., Salamanca, M., Diaz-Corrales, J.D., Flórez, E., Silva-Agredo, J. and Torres-Palma, R.A. (2021). Understanding the removal of an anionic dye in textile wastewater by adsorption on ZnCl2 activated carbons from rice and coffee husk wastes: A combined experimental and theoretical study. *Journal of environmental chemical engineering, 9*, 105685. https://doi.org/10.1016/j.jece.2021.105685

[26] Prasanna, K. (2022). A novel adsorption process for the removal of salt and dye from saline textile industrial wastewater using a three-stage reactor with surface modified adsorbents. *Journal of environmental chemical engineering, 10*, 108729. https://doi.org/10.1016/j.jece.2022.108729

[27] Ssouni, S., Miyah, Y., Benjelloun, M., Mejbar, F., El-Habacha, M., Iaich, S., Addi, A.A. and Lahrichi, A. (2023). High-performance of muscovite clay for toxic dyes' removal: Adsorption mechanism, response surface approach, regeneration, and phytotoxicity assessment. *Case studies in chemical and environmental engineering, 8*, 100456.

https://doi.org/10.1016/j.cscee.2023.100456

[28] Özacar, M., Şengil, İ. A., Türkmenler, H. (2008). Equilibrium and kinetic data, and adsorption mechanism for adsorption of lead onto valonia tannin resin. *Chemical engineering journal*, *143*(1-3), 32-42. https://doi.org/10.1016/j.cej.2007.12.005.

[29] Shakir, I. K. (2010). Kinetic and isotherm modeling of adsorption of dyes onto sawdust. *Iraqi journal of chemical and petroleum engineering*, *11*(2), 15-27. https://doi.org/10.31699/IJCPE.

[30] Duran, C., Ozdes, D., Gundogdu, A., Senturk, H. B. (2011). Kinetics and isotherm analysis of basic dyes adsorption onto almond shell (Prunus dulcis) as a low-cost adsorbent. *Journal of chemical and engineering data*, *56*(5), 2136-2147. https://doi.org/10.1021/je101204j.

[31] Meroufel, B., Benali, O., Benyahia, M., Benmoussa, Y., Zenasni, M. A. (2013). Adsorptive removal of anionic dye from aqueous solutions by Algerian kaolin: Characteristics, isotherm, kinetic and thermodynamic studies. *Journal of materials and environmental science*, *4*(3), 482-491.

[32] Putro, J. N., Santoso, S. P., Soetaredjo, F. E., Ismadji, S., Ju, Y. H. (2019). Nanocrystalline cellulose from waste paper: adsorbent for azo dyes removal. *Environmental nanotechnology, monitoring and management*, *12*, 100260. https://doi.org/10.1016/j.enmm.2019.100260.

[33] Guler, U. A., Sarioglu, M. (2014). Removal of tetracycline from wastewater using pumice stone: equilibrium, kinetic and thermodynamic studies. *Journal of environmental health science and engineering*, *12*, 1-11. https://doi.org/10.1186/2052-336X-12-79.

[34] Zhang, S., Lu, Y., Lin, X., Su, X., Zhang, Y. (2014). Removal of fluoride from groundwater by adsorption onto La (III)-Al (III) loaded scoria adsorbent. *Applied srface science*, *303*, 1-5. https://doi.org/10.1016/j.apsusc.2014.01.169.

[35] Ofomaja, A. E., Naidoo, E. B., Pholosi, A. (2020). Intraparticle diffusion of Cr (VI) through biomass and magnetite coated biomass: A comparative kinetic and diffusion study. *South African journal of chemical engineering*, *32*(1), 39-55. https://doi.org/10.1016/j.sajce.2020.01.005.

[36] Inyang, H.I. Onwawoma, A., Bae, S. (2016). The Elovich equation as a predictor of lead and cadmium sorption rates on contaminant barrier minerals, *Soil Tillage research., 155*, 124–132. https://doi.org/10.1016/j.still.2015.07.013.

[37] Wu, F. C., Tseng, R. L., Juang, R. S. (2009). Characteristics of Elovich equation used for the analysis of adsorption kinetics in dye-chitosan systems. *Chemical engineering journal*, *150*(2-3), 366-373. https://doi.org/10.1016/j.cej.2009.01.014

[38] Zhang, W., Zhang, J., Jiang, Q., Xia, W. (2012). Physicochemical and structural characteristics of chitosan nanopowders prepared by ultrafine milling, *Carbohydrate. polymers. 87*, 309–313. https://doi.org/10.1016/j.carbpol.2011.07.057

[39] Jeong, K., Tatami, J., Iijima, M., Takahashi, T. (2016). Pulverization of Y_2O_3 nanoparticles by using nanocomposite particles prepared by mechanical treatment. *Journal of Asian ceramic societies*, *4*(3), 351-356. https://doi.org/10.1016/j.jascer.2016.06.005

[40] Hashaikeh, R. (2018). Insight into ball milling for size reduction and nanoparticles production of HY zeolite. *Materials chemistry and physics*, *220*, 322-330. https://doi.org/10.1016/j.matchemphys.2018.08.080

[41] Ambroz, F., Macdonald, T. J., Martis, V., Parkin, I. P. (2018). Evaluation of the BET Theory for the Characterization of Meso and Microporous MOFs, *Small methods, 2*, 1800173. https://doi.org/10.1002/smtd.201800173

[42] Zemnukhova, L. A., Panasenko, A. E., Artem'yanov, A. P., Tsoy, E. A. (2015). Dependence of Porosity of Amorphous Silicon Dioxide Prepared from Rice Straw on Plant Variety, *BioResources, 10*(2), 3713–3723. https://doi.org/10.15376/biores.10.2.3713-3723

[43] Samadi-Maybodi, A., Atashbozorg, E. (2006). Quantitative and qualitative studies of silica in different rice samples grown in north of Iran using UV–vis, XRD and IR spectroscopy techniques, Talanta. 70, 756–760. https://doi.org/10.1016/j.talanta.2006.02.004

[44] Mansouri, N., Rikhtegar, N., Panahi, H. A., Atabi, F., Shahraki, B. K. (2013). Porosity,

characterization and structural properties of natural zeolite-clinoptilolite-as a sorbent. *Environment protection engineering*, *39*(1), 139-152.
https://doi.org/10.5277/EPE130111

[45] Castaldi, P., Santona, L., Enzo, S., Melis, P. (2008). Sorption processes and XRD analysis of a natural zeolite exchanged with Pb2+, Cd2+ and Zn2+ cations. *Journal of hazardous materials*, *156*(1-3), 428-434.
https://doi.org/10.1016/j.jhazmat.2007.12.040

[46] Wahyuni, E., Alharrisa, E., Lestari, N., Suherman, S. (2022). Modified waste polystyrene as a novel adsorbent for removal of methylene blue from aqueous media. *Advances in environmental technology, 8*(2), 83-92.
https://doi.org/10.22104/aet.2022.5420.1465

[47] Safari, G. H., Zarrabi, M., Hoseini, M., Kamani, H., Jaafari, J., Mahvi, A. H. (2015). Trends of natural and acid-engineered pumice onto phosphorus ions in aquatic environment: adsorbent preparation, characterization, and kinetic and equilibrium modeling, *Desalination water treat., 54*, 3031–3043.
https://doi.org/10.1080/19443994.2014.915385

[48] Depci, T., Efe, T., Tapan, M., Özvan, A., Aclan, M., Uner, T. (2012). Chemical characterization of Patnos Scoria (Ağrı, Turkey) and its usability for production of blended cement. *Physicochem. problem. miner. process*, *48*(1), 303-315.

[49] Li, K. M., Jiang, J. G., Tian, S. C., Chen, X. J., Yan, F. (2014). Influence of silica types on synthesis and performance of amine–silica hybrid materials used for CO_2 capture. *The journal of physical chemistry C*,*118*(5), 2454-2462.
https://doi.org/10.1021/jp408354r

[50] Gharbani, P., nojavan, A. (2017). Response surface methodology for optimizing adsorption process parameters of reactive blue 21 onto modified kaolin. *Advances in environmental technology, 3*(2), 89-98.
https://doi.org/10.22104/aet.2017.505

[51] Datta, S., Mahapatra, N., Halder, M. (2013). pH-insensitive electrostatic interaction of carmoisine with two serum proteins: A possible caution on its uses in food and pharmaceutical industry. *Journal of photochemistry and photobiology B: Biology*, *124*, 50-62.
https://doi.org/10.1016/j.jphotobiol.2013.04.004

[52] Nazar, M. F., Murtaza, S., Ijaz, B., Asfaq, M., Mohsin, M. A. (2015). Photophysical investigations of carmoisine interacting with conventional cationic surfactants under different pH conditions. *Journal of dispersion science and technology*, *36*(1), 18-27.
https://doi.org/10.1080/01932691.2014.884465

[53] Sadeghi, A., Ehrampoush, M. H., Ghaneian, M. T., Najafpoor, A. A., Fallahzadeh, H., Bonyadi, Z. (2019). The effect of diazinon on the removal of carmoisine by Saccharomyces cerevisiae, *Desalination water treat., 137*, 273–278.
https://doi.org/10.5004/dwt.2019.23189

[54] Behrens, S. H., Grier, D. G. (2001). The charge of glass and silica surfaces. *The Journal of chemical physics*, *115*(14), 6716-6721.
https://doi.org/10.1063/1.1404988

[55] Dove, P. M., Craven, C. M. (2005). Surface charge density on silica in alkali and alkaline earth chloride electrolyte solutions. *Geochimica et cosmochimica acta*, *69*(21), 4963-4970.
https://doi.org/10.1016/j.gca.2005.05.006

[56] Goyne, K. W., Zimmerman, A. R., Newalkar, B. L., Komarneni, S., Brantley, S. L., Chorover, J. (2002). Surface charge of variable porosity Al_2O_3 (s) and SiO_2 (s) adsorbents. *Journal of porous materials*, *9*, 243-256.
https://doi.org/10.1023/A:1021631827398.

[57] Scott, R. P. (1980). The silica-gel surface and its interactions with solvent and solute in liquid chromatography. In *faraday symposia of the chemical society* (Vol. 15, pp. 49-68). Royal society of chemistry.
https://doi.org/10.1039/fs9801500049

[58] Rawat, A. P., Singh, D. P. (2018). Decolourization of malachite green dye by mentha plant biochar (MPB): a combined action of adsorption and electrochemical reduction processes. *Water science and technology*, *77*(6), 1734-1743.
https://doi.org/10.2166/wst.2018.059

[59] Song, J., Kim, M. W. (2010). Second harmonic generation study of malachite green

adsorption at the interface between air and an electrolyte solution: observing the effect of excess electrical charge density at the interface. *The journal of physical chemistry B*, *114*(9), 3236-3241. https://doi.org/10.1021/jp9104882

[60] Özacar, M., Şengil, İ. A. (2005). Adsorption of metal complex dyes from aqueous solutions by pine sawdust. *Bioresource technology*, *96*(7), 791-795. https://doi.org/10.1016/j.biortech.2004.07.011

[61] Bhattacharyya, K. G., Sharma, A. (2004). Adsorption of Pb (II) from aqueous solution by Azadirachta indica (Neem) leaf powder. *Journal of hazardous materials*, *113*(1-3), 97-109. https://doi.org/10.1016/j.jhazmat.2004.05.034

[62] Özacar, M. (2003). Adsorption of phosphate from aqueous solution onto alunite, *Chemosphere*. *51*, 321–327. https://doi.org/10.1016/S0045-6535(02)00847-0

[63] Özacar, M., Şengil, İ. A. (2003). Adsorption of reactive dyes on calcined alunite from aqueous solutions. *Journal of hazardous materials*, *98*(1-3), 211-224. https://doi.org/10.1016/S0304-3894(02)00358-8

How to site this paper:

Bahman, P., Bagheri lotfabad, T., Heydarinasab, A., & Yaghmaei, S. (2024). Adsorption of Carmoisine and Malachite Green on Silicon Dioxide-based Stones Nanosized by Ball Milling. Advances in Environmental Technology, 10(2), 142-159. doi: 10.22104/aet.2024.6740.1840